

Molecular beam epitaxy based growth of cubic GaN quantum dots

T. Schupp^{*1}, T. Meisch², B. Neuschl², M. Feneberg², K. Thonke², K. Lischka¹, and D. J. As¹

¹ Universität Paderborn, Department Physik, Warburger Str. 100, 33095 Paderborn, Germany

² Institut für Quantenmaterie, Gruppe Halbleiterphysik, Universität Ulm, 89069 Ulm, Germany

Received 1 September 2010, accepted 21 October 2010

Published online 17 March 2011

Keywords molecular beam epitaxy, nitrides, quantum dots

* Corresponding author: e-mail Thorsten.Schupp@uni-paderborn.de, Phone: +49 5251 60 5831, Fax: +49 5251 60 5843

Zinc-blende GaN/AlN quantum dots were grown in a molecular beam epitaxy system by two alternative methods. In method A the quantum dots were formed by the Stranski-Krastanov process, whereas in method B the quantum dots were created by a vapor-liquid-solid process, respectively. The density of the Stranski-Krastanov quantum dots was adjustable in a range of $5 \times 10^9 \text{ cm}^{-2}$ to $5 \times 10^{12} \text{ cm}^{-2}$.

The density of the quantum dots grown by method B was controllable in the range of $5 \times 10^8 \text{ cm}^{-2}$ to $5 \times 10^{12} \text{ cm}^{-2}$. For both methods the samples with a high density of quantum dots have shown strong optical activity in photoluminescence spectroscopy. The emission energy of the quantum dots was tuneable in a range of 3.5 eV to 3.9 eV by alteration of the quantum dot height.

© 2011 WILEY-VCH Verlag GmbH & Co. KGaA, Weinheim

1 Introduction With the ongoing commercial success of nitride based light emitting diodes, a growing interest in wide-bandgap quantum dots (QDs) can be observed. The realization of optical and quantum optical devices based on group-III nitride QDs seems to be the next logical step. Long electron spin relaxation times are of great interest for spin-based semiconductor electronics. The Dyakonov–Perel spin relaxation mechanism is based on an intrinsic conduction-band spin splitting caused by spin-orbit coupling (SOC) [1]. Wide-gap semiconductors like GaN have weak SOC compared to GaAs. However, the wurtzite structure of hexagonal GaN (h-GaN) contributes to the spin splitting, leading to intrinsic short spin lifetimes [2]. In contrast, zinc-blende (cubic) phase GaN (c-GaN) combines the benefits of the high cubic symmetry and small SOC. Accordingly, long exciton spin lifetimes in c-GaN QDs exceeding 10 ns have been reported [3]. Furthermore, for h-GaN QDs, single photon emitters have been realized, showing photon antibunching and triggered single-photon generation [4]. However, the Quantum Confined Stark Effect caused by internal electric fields leads to a reduced recombination probability of electrons and holes in confined states. As a result, the long radiative recombination time leads to low repetition rate photonic devices. The metastable zinc-blende (cubic) phase of AlN (c-AlN) and GaN has no polarization fields in (001) growth direction [5]. Consequently, the radiative recombination rate of c-GaN QDs

was measured to be two orders of magnitude higher than the recombination rate of h-GaN QDs [6].

We report on two alternative methods to grow c-GaN QDs. In method A the Stranski-Krastanov (SK) growth process is utilized to create QDs. Stranski-Krastanov QDs are formed by strain induced islanding in lattice-mismatched heteroepitaxy [7]. In method B a vapor-liquid-solid process, namely droplet epitaxy (DE), is applied. Here, liquid Ga droplets are formed and nitridated to create QDs [8]. With DE the size and density of the QDs can be controlled over a wide range from 10^8 cm^{-2} to 10^{12} cm^{-2} . By variation of the quantum dot height the emission energy of the quantum dots is tunable in a wide range of 3.5 eV to 3.9 eV.

2 Experimental procedure The c-GaN QDs were embedded in 3C-AlN (001) barrier layers on 3C-SiC (001) substrate. The growth was carried out in a Riber 32 MBE system, including an Oxford Instruments N plasma cell and standard Ga and Al effusion cells. In-situ growth monitoring was achieved by reflection high energy electron diffraction (RHEED). Atomic force microscopy (AFM) was utilized to analyze the surface structure of the grown layers and QDs. To obtain optical data, photoluminescence (PL) spectroscopy was carried out. The samples were excited by an ArF excimer laser with $\lambda=193\text{nm}$. The PL was detected by a liquid nitrogen cooled charge coupled device camera mounted to a grating monochromator with a focal length of

© 2011 WILEY-VCH Verlag GmbH & Co. KGaA, Weinheim

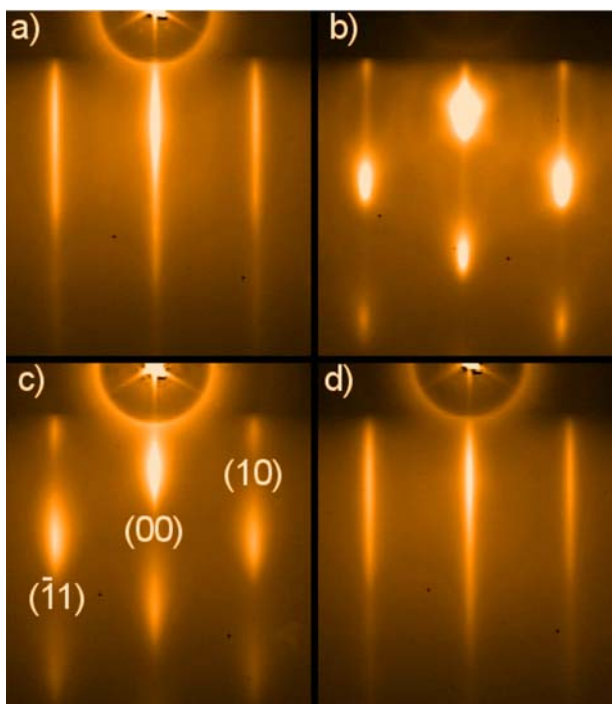


Figure 1 RHEED patterns: (a) Reflections of the c-AlN layer, long thin streaks indicate a smooth 2D surface. (b) Reflections of c-GaN SK QDs, the spotty reflections indicate 3D islands of cubic crystal structure. (c) Reflections of c-GaN droplet QDs. (d) Reflections of the c-AlN after 30 ML QD overgrowth

1 m. The samples were mounted in a temperature controllable liquid helium cryostat to allow for PL investigations at different temperatures.

3 Results and discussion

3.1 Growth The first step is the cleaning of the 3C-SiC substrate by an Al deposition and desorption process, followed by the growth of a 30 nm thick c-AlN barrier layer at 730 °C substrate temperature by plasma assisted molecular beam epitaxy (PAMBE) [9]. The RHEED pattern of the AlN surface in Fig. 1(a) shows long thin streaks indicating a smooth two-dimensional surface [10]. The atomically smooth AlN surface is verified by AFM. For the fabrication of SK QDs the strain energy is of great importance [7]. Cubic AlN is pseudomorphically strained on 3C-SiC and has a lateral lattice parameter of $a=4.36 \text{ \AA}$. The lattice misfit between the barrier layer and the c-GaN ($a=4.50 \text{ \AA}$) is 3.2% [11,12]. The initial GaN monolayers (ML) are grown pseudomorphically strained on c-AlN. Once the critical thickness of 2 ML is reached, the layer is transformed into SK QDs driven by strain relaxation. The density and size of the SK GaN QDs is controlled by the deposition of the equivalent of 2 to 12 ML of GaN on the AlN layer. Figure 1(b) shows the RHEED pattern after the formation of the GaN SK QDs. Resulting from an electron

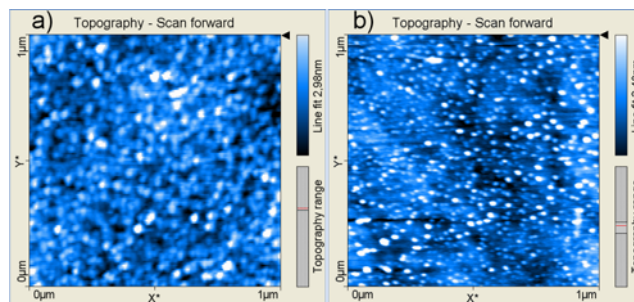


Figure 2 Atomic force microscopy images: (a) $1 \times 1 \mu\text{m}^2$ area of the AlN surface covered with SK GaN QDs. The average width of the QDs is 25 nm, the height 3 nm and the density $1 \times 10^{11} \text{ cm}^{-2}$, (b) $1 \times 1 \mu\text{m}^2$ area of the AlN surface covered with DE GaN QDs. The average width of the QDs is 15 nm, the height 2.5 nm and the density $3 \times 10^{10} \text{ cm}^{-2}$.

transmission component through three dimensional islands, the spotty reflections are an indication of quantum dots on the surface [10].

The fabrication of the c-GaN DE QDs begins with the deposition of a defined amount of Ga, equivalent to 1-12 ML. The formation of Ga droplets is induced by the strong cohesion force between the Ga atoms. The distance between the Ga droplets is governed by two main factors, the amount of deposited Ga and by the surface diffusion length, the latter controlled by the substrate temperature [8]. For this sample series an AlN surface temperature of 350 °C was used. In the next step the Ga droplets are nitridated by exposure to the N plasma beam for 3 to 15 minutes while ramping up the substrate temperature from 350 °C to 730 °C. Figure 1(c) shows the RHEED pattern after the nitridation of the Ga droplets. Similar to the case of SK QDs spotty reflections indicate quantum dots on the surface. As all reflections in the RHEED pattern can be attributed to the zinc-blende lattice structure, cubic phase purity can be concluded within detection limits [13].

In the final step the c-GaN QDs are overgrown by a 30 nm c-AlN barrier layer at 730 °C substrate temperature. Figure 1(d) shows the RHEED pattern of the AlN surface after QD overgrowth with long thin streaks and the absence of spotty reflections. As a result, a smooth surface with full epitaxial overgrowth of the GaN QDs can be followed. AFM verifies the smooth AlN surface after GaN QD overgrowth.

3.2 Atomic force microscopy We determined the size of the QDs and the distribution on the surface by AFM of uncapped GaN QDs. Figure 2(a) shows an AFM image of a $1 \times 1 \mu\text{m}^2$ area of the AlN surface covered with SK GaN QDs. The average width of the QDs is 25 nm, the height 3 nm and the density $1 \times 10^{11} \text{ cm}^{-2}$. The high density is typical for SK QDs, as SK QDs can only be formed after the critical thickness amount of GaN has been deposited. However, for DE the limitation to high densities does not apply. Figure 2(b) shows an AFM image of GaN DE QDs

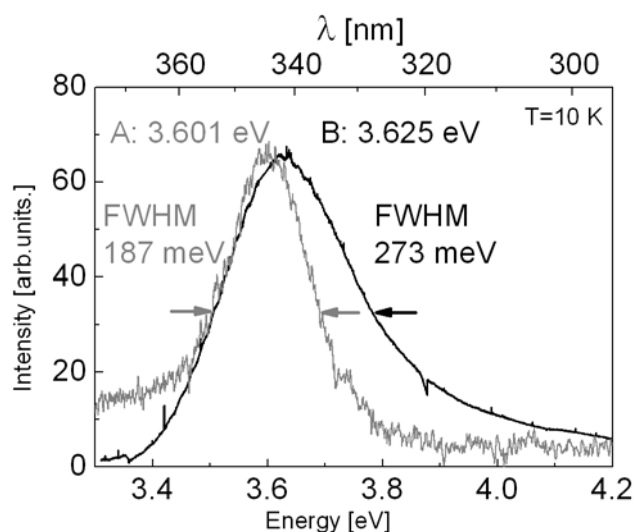


Figure 3 Photoluminescence spectra: (A) Gaussian shaped emission band of c-GaN SK QDs peaking at an energy of 3.601 ± 0.01 eV. FWHM 187 meV. (B) Gaussian shaped emission band of c-GaN DE QDs peaking at an energy of 3.625 ± 0.01 eV, FWHM 273 meV. A high energy tail indicates a skewed size distribution towards smaller QDs.

of medium density. The average width of the QDs is 15 nm, the height 2.5 nm and the density $3 \times 10^{10} \text{ cm}^{-2}$. Compared to SK QDs the size distribution is significantly larger.

3.3 Photoluminescence spectroscopy The photoluminescence spectrum of a single QD ideally has very narrow atom-like spectral lines, much narrower than the broad emission bands observed for bulk material. The superposition of all QDs emission delta peaks forms the emission band of a given sample as a whole. The ensemble of QDs excited by the ArF laser is in the order of 10^8 QDs, consequently the shape of the emission is correlated to the size distribution of the QDs. Earlier research on SK c-GaN QDs has shown, that the determining factor for the QD emission energy is the height of the QD [14]. To analyze these aspects, comparable samples with and without 30 nm AlN cap layer have been grown, as capped QDs cannot be measured by AFM and uncapped QDs did not show PL. Overview PL spectra were taken in the energy range from 3 eV to 6 eV, but as no PL luminescence was observed above 4.5 eV, the high resolution spectra were measured up to 4.5 eV. The 10 K PL spectrum of a c-GaN SK QD sample with 8 ML of deposited GaN can be seen in Fig. 3 (the gray curve marked with the letter A). A Gaussian shaped emission band with an intensity maximum at an energy of 3.601 ± 0.01 eV and a full width at half maximum (FWHM) of 187 meV can be identified. The average height of the uncapped QDs, measured by AFM, is $3.3 \text{ nm} \pm 0.2 \text{ nm}$. The theoretical work of Fonoberov et al. on c-GaN QDs predicts an exciton ground state transition energy of 3.59 eV for QDs having a dot height of 3.3 nm above the wetting layer [14]. This energy is in good

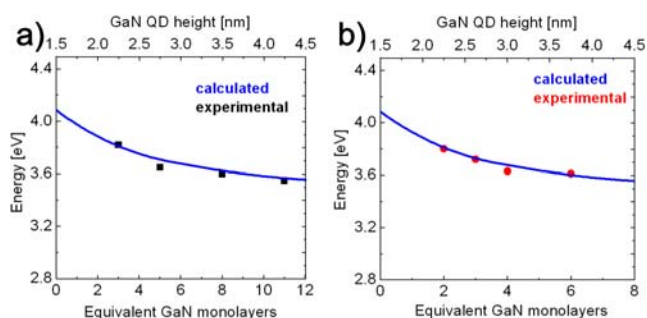


Figure 4 Correlation between deposited GaN amount, QD height, and QD emission energy. The dots mark the measured QD emission energies of 4 samples. The Graph shows the calculated QD emission energy over QD height relation; (a) shows the relationship for c-GaN SK QDs, (b) shows the relationship for c-GaN DE QDs.

agreement with the measured energy peak at 3.60 eV of the capped c-GaN SK QDs.

The PL spectrum of a c-GaN DE QD sample with the equivalent of 4 ML of deposited GaN at a temperature of 10 K can be seen in the black curve in Fig. 3, marked with the letter B. An emission band with an intensity maximum at an energy of 3.625 ± 0.01 eV and a FWHM of 273 meV can be identified. Moreover, a high energy tail indicates a skewed size distribution towards smaller QDs. AFM measurements reveal an average height of the uncapped DE QDs of 3.1 nm. Calculations based on c-GaN SK QDs for a QD height of 3.1 nm above the wetting layer result in an exciton ground state transition energy of 3.62 eV [14]. Thus, the measured emission energy is in good agreement with the calculation.

To investigate the relationship between the deposited GaN amount, the QD height and the QD emission energy a series of samples with varying deposited GaN amount has been grown for c-GaN SK QDs and c-GaN DE QDs, respectively. The PL spectra of the SK QDs samples show a decrease of emission energy from 3.82 eV to 3.55 eV with increasing GaN deposition from 3 to 11 ML, as shown by the dots in Fig. 4(a). For DE QDs, the PL spectra show a decrease of emission energy from 3.80 eV to 3.61 eV with increasing GaN deposition from 2 to 6 ML, as shown by the dots in Fig. 4(b). A Comparison of the deposited GaN amount with the AFM measured QD height reveals a correlation for both QD types. Accordingly, a relationship between the QD height and the emission energy can be followed. This relationship is shown in Fig. 4(a) for SK QDs and Fig. 4(b) for DE QDs, the measured dots are in good agreement with the calculated curve of the QD emission energies in dependence of the QD height [14]. As a result, the emission energy of a QDs sample can be adjusted by the amount of deposited GaN.

4 Conclusion Phase-pure zinc-blende GaN quantum dots were grown on 3C-AlN(001) by two different methods. The Stranski-Krastanov growth process yielded c-

GaN QDs of high density and narrow size distribution. The droplet epitaxy method showed broader size distribution, mainly because of a tail towards smaller QDs. However, DE allowed to grow c-GaN QDs in a wider range of densities down to 10^8 cm^{-2} . Depositing an equal amount of GaN for both QD growth methods, the DE QDs were on average higher and showed lower emission energy than the SK QDs. Comparing QDs of the two types with the same height revealed an equal emission energy. As a result, the correlation of QD height and emission energy holds for both types of QDs and is in agreement with calculations made by Fonoberov et al. [14]. For both methods the emission energy of the quantum dots was tunable in a wide range by alteration of the quantum dot height.

Acknowledgement This work was supported by the DFG graduate program GRK 1464 “Micro- and Nanostructures in Optoelectronics and Photonics”. We would like to thank Dr. M. Abe and Dr. H. Nagasawa of HOYA Corporation for supplying the 3C-SiC substrates.

References

- [1] M. I. Dyakonov and V. I. Perel, *Sov. Phys. Solid State* **13**, 3023 (1972).
- [2] J. H. Buß, J. Rudolph, F. Natali, F. Semond, and D. Hägele, *Phys. Rev. B* **81**, 155216 (2010).
- [3] D. Lagarde, A. Balocchi, H. Carrère, P. Renucci, T. A. X. Marie, S. Founta, and H. Mariette, *Phys. Rev. B* **77**, 041304 (2008).
- [4] C. Santori, S. Götzinger, Y. Yamamoto, S. Kako, K. Hushino, and Y. Arakawa, *Appl. Phys. Lett.* **87**, 051916 (2005).
- [5] D.J. As, *Microelectron. J.* **40**, 204 (2009).
- [6] J. Simon, N. T. Pelekanos, C. Adelman, E. Martinez-Guerrero, R. André, B. Daudin, Le Si Dang, and H. Mariette, *Phys. Rev. B* **68**, 035312 (2003).
- [7] E. Martinez-Guerrero, F. Chabuel, B. Daudin, J. L. Rouviere, and H. Mariette, *Appl. Phys. Lett.* **81**, 5117 (2002).
- [8] T. Schupp, T. Meisch, B. Neuschl, M. Feneberg, K. Thonke, K. Lischka, and D. J. As, *J. Cryst. Growth*, in press (2010).
- [9] T. Schupp, K. Lischka, and D. J. As, *J. Cryst. Growth* **312**, 1500 (2010).
- [10] W. Braun, *Applied RHEED*, Springer Tracts in Modern Physics, Vol. 154 (Springer, Berlin, 1999).
- [11] A. Taylor and R. M. Jones, *Silicon Carbide - A High Temperature Semiconductor*, edited by J. R. O'Connor (Pergamon Press, Oxford, 1960), p. 147.
- [12] S. Strite, J. Ruan, Z. Li, A. Salvador, H. Chen, D. J. Smith, W. J. Choyke, and H. Morko, *J. Vac. Sci. Technol. B* **9**, 1924 (1991).
- [13] S. Sanorpim, E. Takuma, H. Ichinose, R. Katayama, and K. Onabe, *Phys. Status Solidi B* **244**, 1769 (2007).
- [14] V. A. Fonoberov and A. A. Balandin, *J. Appl. Phys.* **94**, 7178 (2003).